Available online at www.sciencedirect.com
SCIENCE DIRECT®
Journal of Sound and Vibration 266 (2003) 147–170
JOURNAL OF SOUND AND VIBRATION
www.elsevier.com/locate/jsvi

Impacts of structural–acoustic coupling on the performance of energy density-based active sound transmission control

S.K. Lau, S.K. Tang*

Department of Building Services Engineering, The Hong Kong Polytechnic University, Hung Hom Kowloon, Hong Kong, People's Republic of China

Received 22 January 2002; accepted 6 September 2002

Abstract

This paper investigates numerically the performance of the active sound transmission control into a rectangular cavity through a flexible panel under the energy density-based error-sensing algorithm. Full coupling between the sound transmitting panel and the enclosed space is considered. A pure vibration actuator, a pure acoustic source and a combined control source system are used as the secondary control source in the active control and their performances are studied. Formulae for the coupled eigenfrequencies of the cavity and the flexible panel are also derived. The strength of the structural–acoustic coupling, the ratio between the first eigenfrequencies of the cavity and the panel and the difference between the excitation frequency and the coupled eigenfrequencies, especially the latter, are found to have crucial impacts on the performance of the active control regardless the type of control source used.

1. Introduction

Low-frequency sound transmission through thin panels or weak structures, such as windows and partition walls, is a problem commonly found in buildings. Traditional passive control methods for sound transmission are to damp and/or stiffen the weak structures, which are only effective at high frequencies. In the past two decades, some researchers have switched their interest in controlling this unwanted sound transmission to the rooms by active means [1–10]. They have proved that the active noise control (ANC) method is effective in controlling low-frequency sound inside an enclosed space.

*Corresponding author. Tel.: +852-2766-5847; fax: +852-2774-6146.
E-mail address: besktang@polyu.edu.hk (S.K. Tang).

0022-460X/03/$ - see front matter
doi:10.1016/S0022-460X(02)01295-6

The idea of active sound transmission control was first proposed by Fuller and Jones [1]. They applied the active structural acoustic control (ASAC), using a force actuator, on a cylindrical shell, aiming at alleviating the noise transmitted into the fuselage from the jet engines. Since then, many studies were concentrated on the ASAC [2–10]. Pan et al. [2–4] analyzed the ASAC on a flexible panel of a rectangular cavity using potential energy control. Two modes of control are concluded [2–4]. They are the panel-controlled modes, in which the energy transmission is from one dominating structural mode into several acoustic modes, and cavity-controlled modes in which the energy transmission is from several structural modes into one dominating acoustic mode. These two control modes are in general co-existing [5]. Recently, the study of ASAC has extended to include the use of structural error sensors such as accelerometers [6] and polyvinylidene fluoride material [7].

ASAC with the potential energy error sensing is effective at some panel-controlled modes and a few cavity-controlled modes for weak structural–acoustic coupling [8]. However, it has the disadvantage of producing significant increase of the flexible panel kinetic energy at cavity-controlled mode frequencies [8]. Also, the force actuators and structural sensors on the weak structures have limitations in their applications. For example, such sensors mounted on windows will obstruct the line of sight and thus is undesirable. Acoustic sound transmission control using secondary acoustic sources inside the cavity can eliminate the large increase of the kinetic energy of flexible panel [8] and is worthwhile to study due to its effectiveness in controlling the cavity-controlled modes. Snyder and Hansen [9,10] and Kim and Brennan [8] have considered the combined control source system (i.e., using force and acoustic actuators simultaneously) in order to control both the panel-controlled and cavity-controlled modes. Weak structural–acoustic coupled systems were studied. However, the influence of strong structural–acoustic coupling on active sound transmission control is not well documented.

For error-sensing control algorithms, the potential energy and squared pressure sensing techniques have been studied extensively [2–5,8–10]. However, they have their inherited shortcomings. Potential energy control is the theoretical optimized solution for global control of an enclosed sound field. However, it is difficult to implement, as a large amount of sound pressure sensors are practically required. For squared pressure control, global control of an enclosed sound field is only possible at frequencies far below the first eigenfrequency of the cavity, while only a confined quiet zone around the error-sensing point can be achieved at other frequencies [11]. Discrete quiet and amplification zones, as well as highly non-uniform sound fields, are also observed at high frequencies [11]. Also, two adverse effects of spillovers and detrimental effects occur, resulting in largely amplified sound pressures throughout the cavity except the error-sensing points if the error-sensing microphone is not located properly [11].

Sommerfeldt and Nashif [12,13] proposed the energy density control (minimizing acoustic energy densities at discrete locations) in hope of a system with a more effective global sound field control and a performance less dependent on error sensor locations. Lau and Tang [11] has shown the effectiveness of this energy density control inside a slightly damped rectangular cavity with sound field visualization. Energy density control has the advantages of eliminating the spillovers and detrimental effects observed under the squared pressure control, as well as producing a more uniform sound. The performance of the energy density control is much closer to that of the potential energy control when compared with that obtained under the squared pressure control.

This paper documents a study of the effectiveness of controlling sound transmission through a flexible panel into a rectangular cavity using the energy density-based active control. Full couplings between the panel vibration and room acoustic modes are considered. Two dimensionless parameters related to the mechanical properties of the flexible panel and the cavity are introduced. They are the strength of the structural–acoustic coupling and the ratio between the first eigenfrequencies of the cavity and the panel. The present investigation includes frequencies up to five times the first natural frequencies of the cavity. The performance of the active control under pure vibration, pure acoustic and combined secondary sources are compared. It is hoped that the advantages and weaknesses of each control source method can be found and the results can provide useful information on the use of active control in building acoustics, especially in the low-frequency range.

2. Optimal secondary source strengths

The sound pressure inside an enclosed space and the structural vibration velocity of a flexible panel can be determined by the summation of infinite sets of acoustic and structural modal components, respectively. In matrix form, the vector of sound pressures at the points $\mathbf{x}_i$s inside an enclosed space, $\mathbf{p} = [p(\mathbf{x}_1\omega) \quad p(\mathbf{x}_2\omega) \quad p(\mathbf{x}_3\omega)\dots]^{\mathrm{T}}$, can be written simply as the product of the acoustic mode shape matrix at those points, $\mathbf{\Psi}$, and the complex acoustic pressure modal amplitude vector, $\mathbf{a}$, due to sources, as

$$\mathbf{p} = \mathbf{\Psi}^{\mathrm{H}}\mathbf{a}, \tag{1}$$

where each column of $\mathbf{\Psi}$ consists of N acoustic mode eigenfunctions, $\psi_n(\mathbf{x}_i, \omega)$, at a specified location, $\mathbf{x}_i$, inside the cavity. Similarly, the vector of the structural vibration velocities at the points $\mathbf{y}_i$s on the flexible panel, $\mathbf{u}_s = [u_s(\mathbf{y}_1\omega) \quad u_s(\mathbf{y}_2\omega) \quad u_s(\mathbf{y}_3\omega)\dots]^{\mathrm{T}}$, can be written as the product of the structural mode shape matrix for those points, $\mathbf{\Phi}$, and the complex structural vibration velocity modal amplitude vector, $\mathbf{b}$, as

$$\mathbf{u_s} = \mathbf{\Phi}^{\mathrm{H}}\mathbf{b}, \tag{2}$$

where each column of $\mathbf{\Phi}$ consists of M structural mode eigenfunctions, $\phi_m(\mathbf{y}_i, \omega)$, at a specified location, $\mathbf{y}_i$, on the flexible panel. It can be shown by using the impedance-mobility approach [8] that

$$\mathbf{a} = \mathbf{A}\mathbf{Z}_a(\mathbf{R}_a\mathbf{t}_c + \mathbf{C}\mathbf{Y}_s\mathbf{g}_p) \tag{3a}$$

and

$$\mathbf{b} = \mathbf{B}\mathbf{Y}_s(\mathbf{R}_s\mathbf{t}_c + \mathbf{g}_p). \tag{3b}$$

The concept of the impedance-mobility approach is to present the solutions of the coupled structural–acoustic responses in terms of the compact matrixes for the modal impedance and mobility of the acoustic and structural systems. Details of such approach can be found in the works of Kim [14,15] and are briefly summarized in Appendix A. One can rearrange $\mathbf{a}$ and $\mathbf{b}$ such that

$$\mathbf{a} = \eta_c\mathbf{A}\hat{\mathbf{Z}}_a(\hat{\mathbf{R}}_a\hat{\mathbf{t}}_c + \hat{\mathbf{C}}\hat{\mathbf{Y}}_s\hat{\mathbf{g}}_p), \tag{4a}$$

$$\mathbf{b} = \frac{S_f}{M_s \omega_{sc}} \mathbf{B} \hat{\mathbf{Y}}_s (\hat{\mathbf{R}}_s \hat{\mathbf{t}}_c + \hat{\mathbf{g}}_p), \tag{4b}$$

where

$$\eta_c = \frac{K_a}{M_s \omega_{ac} \omega_{sc}} \tag{5}$$

and all variables in Eqs. (4a) and (4b) are dimensionless except $\mathbf{a}$, $\hat{\mathbf{t}}_c$ and $\hat{\mathbf{g}}_p$, whose units are $\mathrm{N\,m^{-2}}$, and $\mathbf{b}$, S_f, M_s and ω_{sc} whose units are $\mathrm{m\,s^{-1}}$, $\mathrm{m^2}$, kg and $\mathrm{s^{-1}}$, respectively. Therefore, $\hat{\mathbf{Z}}_a$ and $\hat{\mathbf{Y}}_s$ are solely related to the modal characteristics of the cavity and flexible panel respectively. $\hat{\mathbf{R}}_a$ represents the normalized couplings between the control source locations and acoustic modes. The acoustic and vibration source strengths are normalized by $(\omega_{sc} M_s / S_f^2)$ and S_f in $\hat{\mathbf{t}}_c$ and $\hat{\mathbf{g}}_p$, respectively, thus they can be easily compared between various combinations of cavity and flexible panel. η_c depends on the medium inside the cavity, and the material and dimension of the cavity and flexible panel (Appendix B). Eqs. (1) and (4a) are the comprehensive equations for acoustic modes and are also useful in finding out the combined effects of sound transmission through flexible panel with internal acoustic sources and/or vibration forces on the panel. Eqs. (2) and (4b) are the comprehensive equations for vibration of flexible panel driven by vibration forces, external and/or internal acoustic fields with the effects of the structural–acoustic coupling included.

Energy density control is a promising algorithm for both global and local noise control inside a cavity [11]. Its strategy is to minimize energy densities at discrete locations inside the cavity. The energy density at a point, $\mathbf{x}_i$, inside a cavity is

$$ED = \frac{1}{2\rho_a c^2} |p(\mathbf{x}_i, \omega)|^2 + \frac{\rho_a}{2} |u_a(\mathbf{x}_i, \omega)|^2, \tag{6}$$

which is the sum of both the acoustic potential and kinetic energy densities at the point concerned. Therefore, the acoustic particle velocities, as well as the acoustic pressures, are also optimized for minimizing energy densities inside the cavity. Substituting Euler's equation $\nabla p(\mathbf{x}, \omega) \approx -\mathrm{j} k \rho_a c u_a(\mathbf{x}, \omega)$, Eqs. (1) and (4a) into Eq. (6), the sum of the energy densities at discrete locations inside the cavity, ED_{sum}, can be written in the form of an Hermitian quadratic expression

$$\begin{aligned} ED_{sum} = \frac{\eta_c^2}{2\rho_a c^2} \Bigg\{ & \hat{\mathbf{t}}_c^{\mathrm{H}} \left[\hat{\mathbf{R}}_a^{\mathrm{H}} \hat{\mathbf{Z}}_a^{\mathrm{H}} \mathbf{A}^{\mathrm{H}} \left(\boldsymbol{\Psi}_e \boldsymbol{\Psi}_e^{\mathrm{H}} + \frac{1}{k^2} \nabla \boldsymbol{\Psi}_e \cdot \nabla \boldsymbol{\Psi}_e^{\mathrm{H}} \right) \mathbf{A} \hat{\mathbf{Z}}_a \hat{\mathbf{R}}_a \right] \hat{\mathbf{t}}_c \\ & + \left[\hat{\mathbf{g}}_p^{\mathrm{H}} \hat{\mathbf{Y}}_s^{\mathrm{H}} \hat{\mathbf{C}}^{\mathrm{H}} \hat{\mathbf{Z}}_a^{\mathrm{H}} \mathbf{A}^{\mathrm{H}} \left(\boldsymbol{\Psi}_e \boldsymbol{\Psi}_e^{\mathrm{H}} + \frac{1}{k^2} \nabla \boldsymbol{\Psi}_e \cdot \nabla \boldsymbol{\Psi}_e^{\mathrm{H}} \right) \mathbf{A} \hat{\mathbf{Z}}_a \hat{\mathbf{R}}_a \right] \hat{\mathbf{t}}_c \\ & + \hat{\mathbf{t}}_c^{\mathrm{H}} \left[\hat{\mathbf{R}}_a^{\mathrm{H}} \hat{\mathbf{Z}}_a^{\mathrm{H}} \mathbf{A}^{\mathrm{H}} \left(\boldsymbol{\Psi}_e \boldsymbol{\Psi}_e^{\mathrm{H}} + \frac{1}{k^2} \nabla \boldsymbol{\Psi}_e \cdot \nabla \boldsymbol{\Psi}_e^{\mathrm{H}} \right) \mathbf{A} \hat{\mathbf{Z}}_a \hat{\mathbf{C}} \hat{\mathbf{Y}}_s \hat{\mathbf{g}}_p \right] \\ & + \left[\hat{\mathbf{g}}_p^{\mathrm{H}} \hat{\mathbf{Y}}_s^{\mathrm{H}} \hat{\mathbf{C}}^{\mathrm{H}} \hat{\mathbf{Z}}_a^{\mathrm{H}} \mathbf{A}^{\mathrm{H}} \left(\boldsymbol{\Psi}_e \boldsymbol{\Psi}_e^{\mathrm{H}} + \frac{1}{k^2} \nabla \boldsymbol{\Psi}_e \cdot \nabla \boldsymbol{\Psi}_e^{\mathrm{H}} \right) \mathbf{A} \hat{\mathbf{Z}}_a \hat{\mathbf{C}} \hat{\mathbf{Y}}_s \hat{\mathbf{g}}_p \right] \Bigg\}, \end{aligned} \tag{7}$$

where $\boldsymbol{\Psi}_e$ consists of the acoustic mode shapes for E error-sensing points. Energy densities, potential energy densities and kinetic energy densities of the acoustic field at any points inside the cavity, in general, decrease exponentially with η_c in the traditional passive sound transmission control. The optimized secondary source strengths of energy density control, $\hat{\mathbf{t}}_c$, can be derived by

minimizing ED_{sum} (Eq. (7))

$$\hat{\mathbf{t}}_c = -\left\{\hat{\mathbf{R}}^{\mathrm{H}}\hat{\mathbf{Z}}_a^{\mathrm{H}}\mathbf{A}^{\mathrm{H}}\left(\boldsymbol{\Psi}_e\boldsymbol{\Psi}_e^{\mathrm{H}} + \frac{1}{k^2}\nabla\boldsymbol{\Psi}_e\cdot\nabla\boldsymbol{\Psi}_e^{\mathrm{H}}\right)\mathbf{A}\hat{\mathbf{Z}}_a\hat{\mathbf{R}}\right\}^{-1} \cdot \mathbf{R}^{\mathrm{H}}\hat{\mathbf{Z}}_a^{\mathrm{H}}\mathbf{A}^{\mathrm{H}}\left(\boldsymbol{\Psi}_e\boldsymbol{\Psi}_e^{\mathrm{H}} + \frac{1}{k^2}\nabla\boldsymbol{\Psi}_e\cdot\nabla\boldsymbol{\Psi}_e^{\mathrm{H}}\right)\mathbf{A}\hat{\mathbf{Z}}_a\hat{\mathbf{C}}\hat{\mathbf{Y}}_s\hat{\mathbf{g}}_p. \tag{8}$$

The optimized secondary source strengths of potential energy [14] and squared pressure control algorithms can be determined by replacing $(\boldsymbol{\Psi}_e\boldsymbol{\Psi}_e^{\mathrm{H}} + (1/k^2)\nabla\boldsymbol{\Psi}_e\cdot\nabla\boldsymbol{\Psi}_e^{\mathrm{H}})$ in Eq. (8) with $\mathbf{I}$ and $(\boldsymbol{\Psi}_e\boldsymbol{\Psi}_e^{\mathrm{H}})$, respectively.

3. Numerical experiments and control modes

Computer simulations were carried out to evaluate the performance of energy density-based active sound transmission control using pure vibration, pure acoustic and combined secondary sources. Fig. 1 shows the rectangular cavity and the co-ordinate system adopted in present study. The dimensions of the cavity, L_{x1} (length)$\times L_{x2}$ (width)$\times L_{x3}$ (height), were chosen in a ratio such that $L_{x1}{:}L_{x2}{:}L_{x3} = 1{:}e/\pi{:}1/\pi$ in order to reduce the number of degenerated acoustic modes [16]. Table 1 shows the normalized frequencies of the first 35 natural acoustic and panel vibration modes. The cavity comprises five acoustically rigid walls and a simply supported flexible panel located at $x2 = 0$. The (n,n) and (m,m) diagonal elements of $\hat{\mathbf{Z}}_a$ and $\hat{\mathbf{Y}}_s$, respectively, can be expressed as

$$\hat{Z}_{a,n} = \frac{\mathrm{j}\hat{\omega}}{\hat{\omega}_n^2 - \hat{\omega}^2 + 2\mathrm{j}\xi_n\hat{\omega}_n\hat{\omega}} \tag{9}$$

and

$$\hat{Y}_{s,m} = \frac{\mathrm{j}\hat{\omega}\varphi}{\hat{\omega}_m^2 - \hat{\omega}^2\varphi^2 + 2\mathrm{j}\zeta_m\hat{\omega}_m\hat{\omega}\varphi}, \tag{10}$$

where

$$\varphi = \omega_{ac}/\omega_{sc} \tag{11}$$

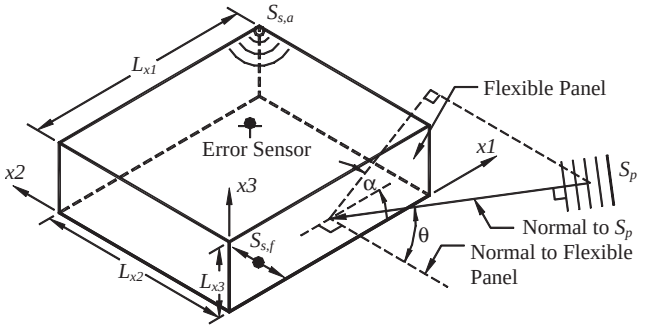

Fig. 1. Schematic diagram for sound transmission and the co-ordinate system adopted.

Table 1
Normalized eigenfrequencies of cavity and panel

Acoustic modes	n	$\hat{\omega}_n$	Structural modes	m	$\hat{\omega}_m$
(1,0,0)	1	1.00	(1,1)	1	1.00
(0,1,0)	2	1.16	(2,1)	2	1.28
(1,1,0)	3	1.53	(3,1)	3	1.74
(2,0,0)	4	2.00	(4,1)	4	2.38
(2,1,0)	5	2.31	(5,1)	5	3.21
(0,2,0)	6	2.31	(1,2)	6	3.72
(1,2,0)	7	2.52	(2,2)	7	4.00
(3,0,0)	8	3.00	(6,1)	8	4.22
(2,2,0)	9	3.06	(3,2)	9	4.46
(0,0,1)	10	3.14	(4,2)	10	5.10
(3,1,0)	11	3.21	(7,1)	11	5.42
(1,0,1)	12	3.30	(5,2)	12	5.93
(0,1,1)	13	3.35	(8,1)	13	6.80
(0,3,0)	14	3.47	(6,2)	14	6.94
(1,1,1)	15	3.49	(7,2)	15	8.14
(1,3,0)	16	3.61	(1,3)	16	8.26
(2,0,1)	17	3.72	(9,1)	17	8.36
(3,2,0)	18	3.79	(2,3)	18	8.54
(2,1,1)	19	3.90	(3,3)	19	9.00
(0,2,1)	20	3.90	(8,2)	20	9.52
(4,0,0)	21	4.00	(4,3)	21	9.64
(2,3,0)	22	4.00	(10,1)	22	10.11
(1,2,1)	23	4.03	(5,3)	23	10.47
(4,1,0)	24	4.16	(9,2)	24	11.08
(3,0,1)	25	4.34	(6,3)	25	11.48
(2,2,1)	26	4.38	(11,1)	26	12.04
(3,1,1)	27	4.50	(7,3)	27	12.68
(3,3,0)	28	4.58	(10,2)	28	12.83
(4,2,0)	29	4.62	(8,3)	29	14.06
(0,4,0)	30	4.62	(12,1)	30	14.16
(0,3,1)	31	4.68	(1,4)	31	14.62
(1,4,0)	32	4.73	(11,2)	32	14.76
(1,3,1)	33	4.78	(2,4)	33	14.90
(3,2,1)	34	4.92	(3,4)	34	15.36
(5,0,0)	35	5.00	(9,3)	35	15.62

The external modal force matrix, $\mathbf{g}_p$, on the flexible panel is induced by an external plane wave S_p. Without loss of generality, the propagation direction of this wave is taken to be at $\theta = \pi/6$ and $\alpha = \pi/4$ in present study. Force control actuator and acoustic control source, when located near to those nodal lines of structural modes and nodal planes of acoustic modes, respectively, do not effectively excite the structural and acoustic modes, respectively. An acoustic mode would be said to be not "controllable" by an acoustic source if the source is placed at a nodal plane of the acoustic mode. The case for controlling a structural mode with a force actuator is similar. The force control actuator, $S_{s,f}$, and acoustic control source, $S_{s,a}$, are located at $(0.495L_{x1}, 0, 0.481L_{x3})$

and (L_{x1}, L_{x2}, L_{x3}), respectively, in order to avoid the nodal points on the structure and inside the cavity throughout the frequency range in present study. The normalized acoustic modal impedance and structural modal mobility in Eqs. (9) and (10) were obtained with acoustic and structural modal damping coefficients (ξ_n and ζ_m, respectively) of 0.01. One thousand one hundred and seventy-three acoustic modes and 522 structural modes are included in the foregoing calculations. The calculations were done using software MATLAB™ on a DEC workstation 600 AU.

Before the analysis of the numerical results, modes for active sound transmission control are discussed in the following sub-sections. It will be shown that the coupled eigenfrequencies are different from those of the natural modes of the panel and the cavity. It will also be illustrated later that their relationships with φ and η_c have great implications on the effectiveness of the active control.

The two parameters, η_c and φ, are critical for passive sound transmission controls. Since the speed of sound and the air density are practically constant, therefore, the traditional measure for controlling sound transmission is to reduce the stiffness K_a/M_s in η_c, so that both the magnitudes of **A** and $\eta_c\hat{\mathbf{Z}}_a\hat{\mathbf{C}}\hat{\mathbf{Y}}_s$ in Eq. (4a) are reduced. This stiffness has been used for describing the structural–acoustic coupling with fixed cavity dimension (for instance, Ref. [15]). In other words, η_c indicates primarily the strength of structural–acoustic coupling in non-resonant condition. The coupling between the panel vibration and the enclosed sound field becomes weaker as η_c gets smaller. For a very weakly coupled system, η_c is very small, **A** and **B** in Eqs. (3) and (4) are approximately equal to **I** [14,15]. Some reductions of sound transmission can also be achieved by adjusting ω_{ac} and ω_{sc} (Eq. 4a). φ indicates how close is the lower order eigenfrequency matching between the panel and the cavity. This is of importance to sound transmission as the problem is more serious in the low-frequency range, especially under damping. Modification of the passive sound transmission control is possible by adjusting φ. φ affects also the active control performance which is expected to be more pronounced at low frequencies. This will be discussed later.

3.1. Panel-controlled modes

The energy transmission from one dominant structural mode of the flexible panel into several acoustic modes of the cavity, can be effectively controlled by suspending the dominant structural mode. Suppose the mth panel vibration mode is the dominant structural mode and the energy is transmitted from this mode to N acoustic modes of the cavity, the complex structural vibration velocity modal amplitudes (Eq. (4b)) can be simplified to

$$\begin{aligned} b_m &= \frac{S_f}{M_s\omega_{sc}}(1+\eta_c\hat{Y}_{s,m}\hat{Z}_{ca,m})^{-1}\hat{Y}_{s,m}(\hat{\mathbf{R}}_{s,m}\hat{\mathbf{t}}_c+\hat{g}_{p,m}) \\ &= \frac{S_f}{M_s\omega_{sc}}\left(\frac{\mathrm{j}\hat{\omega}\varphi}{\hat{\omega}_m^2-\hat{\omega}^2\varphi^2+2\mathrm{j}\zeta_m\hat{\omega}_m\hat{\omega}\varphi+\mathrm{j}\eta_c\hat{Z}_{ca,m}\hat{\omega}\varphi}\right)(\hat{\mathbf{R}}_{s,m}\hat{\mathbf{t}}_c+\hat{g}_{p,m}) \\ &= \frac{S_f}{M_s\omega_{sc}}\hat{Y}_{es,m}(\hat{\mathbf{R}}_{s,m}\hat{\mathbf{t}}_c+\hat{g}_{p,m}), \end{aligned} \tag{12}$$

where

$$\hat{\mathbf{R}}_{s,m} = [\,\mathbf{D}_{f,m} \quad -\eta_c \hat{\mathbf{C}}_m^{\mathrm{T}} \hat{\mathbf{Z}}_a \mathbf{D}_q\,]$$

and

$$\hat{Y}_{es,m} = \frac{\mathrm{j}\hat{\omega}\varphi}{\hat{\omega}_m^2 - \hat{\omega}^2\varphi^2 + 2\mathrm{j}\zeta_m\hat{\omega}_m\hat{\omega}\varphi + \mathrm{j}\eta_c\hat{Z}_{ca,m}\hat{\omega}\varphi}.$$

$\hat{Z}_{ca,m}$ is the normalized coupled acoustic modal impedance due to N acoustic modes of the cavity coupled with the mth structural mode of the flexible panel. $\hat{g}_{p,m}$ is normalized external modal force for the mth structural mode. The formula for $g_{p,m}$ can be found in Roussos [17] and is given in Appendix A for convenience. The criteria for weak coupling of panel-controlled modes [15] can be satisfied when $2\zeta_m\hat{\omega}_m \gg \eta_c|\mathrm{Re}(\hat{Z}_{ca,m})|$ and $\hat{\omega}_m^2 - \hat{\omega}^2\varphi^2 \gg \eta_c|\mathrm{Im}(\hat{Z}_{ca,m})|\hat{\omega}\varphi$, so that $\hat{Y}_{es,m} \approx \hat{Y}_{s,m}$. $|\mathrm{Re}(\hat{Z}_{ca,m})|$ and $|\mathrm{Im}(\hat{Z}_{ca,m})|$ are the normalized acoustic resistant and reactance of the normalized coupled acoustic modal impedance, $\hat{Z}_{ca,m}$, respectively. The coupled eigenfrequency of the flexible panel, $\omega_{c,m}$, can be estimated when the real part of the denominator of $\hat{Y}_{es,m}$ vanishes and is the root of the non-linear equation:

$$\varphi^2\hat{\omega}^2 + \eta_c\,\mathrm{Im}(\hat{Z}_{ca,m})\varphi\hat{\omega} - \hat{\omega}_m^2 = 0. \tag{13}$$

It can be observed from Eq. (12) that the structural vibration velocity amplitudes, and also the acoustic field inside the cavity, get smaller as η_c, $\mathrm{Re}(\hat{Z}_{ca})$, ζ_m, $\hat{\omega}_m$, $\hat{\omega}$ and/or φ increase. The former two parameters relate to the strength and mode of the coupling while the rest are passive parameters.

3.2. Cavity-controlled modes

The cavity-controlled mode refers to the situation where the energy transmission is from several structural modes of the flexible panel to one dominant acoustic mode of the cavity. Suppose the latter is the nth acoustic mode of the cavity and M panel vibration modes are involved, the complex acoustic pressure modal amplitudes can be expressed as

$$\begin{aligned} a_n &= \eta_c(1 + \eta_c\hat{Z}_{a,n}\hat{Y}_{cs,n})^{-1}\hat{Z}_{a,n}(\hat{\mathbf{R}}_{a,n}\hat{\mathbf{t}}_c + \hat{\mathbf{C}}_n\hat{\mathbf{Y}}_s\hat{\mathbf{g}}_p) \\ &= \eta_c\left(\frac{\mathrm{j}\hat{\omega}}{\hat{\omega}_n^2 - \hat{\omega}^2 + 2\mathrm{j}\xi_n\hat{\omega}_n\hat{\omega} + \mathrm{j}\eta_c\hat{Y}_{cs,n}\hat{\omega}}\right)(\hat{\mathbf{R}}_{a,n}\hat{\mathbf{t}}_c + \hat{\mathbf{C}}_n\hat{\mathbf{Y}}_s\hat{\mathbf{g}}_p) \\ &= \eta_c\hat{Z}_{ea,n}(\hat{\mathbf{R}}_{a,n}\hat{\mathbf{t}}_c + \hat{\mathbf{C}}_n\hat{\mathbf{Y}}_s\hat{\mathbf{g}}_p), \end{aligned} \tag{14}$$

where

$$\hat{\mathbf{R}}_{a,n} = [\,\hat{\mathbf{C}}_n\hat{\mathbf{Y}}_s\mathbf{D}_f \quad \mathbf{D}_{q,n}\,] \quad \text{and} \quad \hat{Z}_{ea,n} = \frac{\mathrm{j}\hat{\omega}}{\hat{\omega}_n^2 - \hat{\omega}^2 + 2\mathrm{j}\xi_n\hat{\omega}_n\hat{\omega} + \mathrm{j}\eta_c\hat{Y}_{cs,n}\hat{\omega}}.$$

$\hat{Y}_{cs}$ is the normalized coupled structural modal mobility due to the M panel modes coupled with the nth acoustic mode of the cavity. Also, the criteria for weak coupling [15] of cavity-controlled modes can be satisfied when $2\xi_n\hat{\omega}_n \gg \eta_c|\mathrm{Re}(\hat{Y}_{cs,n})|$ and $\hat{\omega}_n^2 - \hat{\omega}^2 \gg \eta_c|\mathrm{Im}(\hat{Y}_{cs,n})|\hat{\omega}$, so that $\hat{Z}_{ea,n} \approx \hat{Z}_{a,n}$. The coupled eigenfrequency of the cavity, $\omega_{c,n}$, can then be determined when the real part of the

denominator of $\hat{Z}_{ea,n}$ vanishes, that is, when the excitation frequency, $\hat{\omega}$, satisfy the equation

$$\hat{\omega}^2 + \eta_c \,\mathrm{Im}(\hat{Y}_{cs,n})\hat{\omega} - \hat{\omega}_n^2 = 0. \tag{15}$$

For full coupling condition, the acoustic pressure amplitudes inside the cavity decreases as η_c, $\mathrm{Re}(\hat{Y}_{cs})$, ξ_n, $\hat{\omega}_n$ and/or $\hat{\omega}$increase.

3.3. Combined panel- and cavity-controlled modes

Active sound transmission control under combined panel- and cavity-controlled modes will occur at $\hat{\omega} = \hat{\omega}_n = \hat{\omega}_m$ (i.e., $\omega_n = \varphi\omega_m$). Energy transmission is then from one dominant natural structural mode of the flexible panel to one dominant natural acoustic mode of the cavity. Suppose the dominating modes are the mth flexible panel mode and the nth acoustic cavity mode of the cavity, the complex structural vibration velocity and the complex acoustic pressure modal amplitudes can be written as

$$a_{m,n} = \eta_c \hat{Z}_{ea,n}(\hat{\mathbf{R}}_{a,m,n}\hat{\mathbf{t}}_c + \hat{C}_{m,n}\hat{Y}_{s,m}\hat{g}_{p,m}) \tag{16}$$

and

$$b_{m,n} = \frac{S_f}{M_s\omega_{sc}}\,\hat{Y}_{es,m}(\hat{\mathbf{R}}_{s,m,n}\hat{\mathbf{t}}_c + \hat{g}_{p,m}), \tag{17}$$

respectively, where

$$\hat{\mathbf{R}}_{a,m,n} = [\,\hat{C}_{m,n}\hat{Y}_{s,m}\mathbf{D}_{f,m} \quad \mathbf{D}_{q,n}\,] \quad \text{and} \quad \hat{\mathbf{R}}_{s,m,n} = [\mathbf{D}_{f,m} \quad -\eta_c\hat{C}_{m,n}\hat{Z}_{a,n}\mathbf{D}_{q,n}\,].$$

Weakly coupled acoustic pressure and structural vibration velocity amplitudes can be found with $\hat{Z}_{ea,n} \approx \hat{Z}_{a,n}$ and $\hat{Y}_{es,m} \approx \hat{Y}_{s,m}$, where η_c and the mode shape coupling coefficient $\hat{C}_{m,n}$ are small enough to give $2\zeta_m\hat{\omega}_m \gg \eta_c|\mathrm{Re}(\hat{Z}_{ca,m})|$, $\hat{\omega}_m^2 - \hat{\omega}^2\varphi^2 \gg \eta_c|\mathrm{Im}(\hat{Z}_{ca,m})|\hat{\omega}\varphi$, $2\xi_n\hat{\omega}_n \gg \eta_c|\mathrm{Re}(\hat{Y}_{cs,n})|$ and $\hat{\omega}_n^2 - \hat{\omega}^2 \gg \eta_c|\mathrm{Im}(\hat{Y}_{cs,n})|\hat{\omega}$ (Appendix A). The coupled eigenfrequencies of the flexible panel and the cavity can be estimated by using Eqs. (13) and (15), respectively.

4. Total acoustic potential energy attenuation inside cavity

For orthogonal modal characteristic functions, the overall total acoustic potential energy, PE, inside a cavity of volume V, is defined as [18]

$$PE = \frac{V}{4\rho_a c^2}\,\mathbf{a}^{\mathrm{H}}\mathbf{a}, \tag{18}$$

where $\mathbf{a}$ can be found by Eq. (3). One can notice immediately that for the present rectangular enclosure, the total energy obtained by integrating the energy density (Eq. 6) over the volume V is proportional to the PE given by Eq. (18). The attenuation of PE inside the cavity under active control of sound transmission is determined by the difference of PE before and after activating the control. High global control of enclosed sound field possibly exists for high attenuation of PE. Also, PE attenuation is a good indicator for the dominance of quiet zones and amplification zones [11]. In the present study, the performance of active sound transmission control is described by the attenuation of PE under various combinations of the two dimensionless parameters η_c and φ. One

can immediately observe that these two parameters are not independent of each other. Details on how to vary one of them with another fixed are given in Appendix B. Both η_c and φ are logarithmically distributed into 50 intervals in the range $0.01 \leqslant \eta_c \leqslant 1$ and $0.1 \leqslant \varphi \leqslant 10$, giving 2500 different combinations. The frequency concerned is up to $5\omega_{ac}$. The calculations were done at $0.1\omega_{ac}$ intervals. The energy density error sensor is located at ($0.7L_{x1}$, $0.7L_{x2}$, $0.9L_{x3}$). Energy density control is ineffective when the error sensors are located near to the nodal planes of the total energy density field, though the nodal volume of the total energy density field is much less that of the sound field [19]. Also this control algorithm is more effective when the separation between the error sensor and the secondary acoustic source increases, so that the error sensor can obtain the energy density in a relatively uniform and representative region. A detailed investigation of the error sensor location can be found in Lau and Tang [11]. Similar to the results of Lau and Tang [11], the energy density-based control can produce a performance much closer to that under the potential energy control than the squared pressure control in the present study. Therefore, the results obtained using the potential energy and squared pressure control schemes are not presented.

4.1. Pure vibration control

Fig. 2 illustrates the *PE* attenuation maps under the energy density-based active control with pure vibration control source at different values of η_c and φ across the frequency range concerned. These *PE* attenuation maps show a gradual pattern variation with the strength of the structural–acoustic coupling. It can be observed that this control scheme can produce high sound attenuation at frequencies below ω_{ac} for $\varphi \leqslant 1$ regardless the strength of structural–acoustic coupling η_c. Also, η_c basically has negligible effects on the *PE* attenuation at high frequency with $\varphi > 2$, though

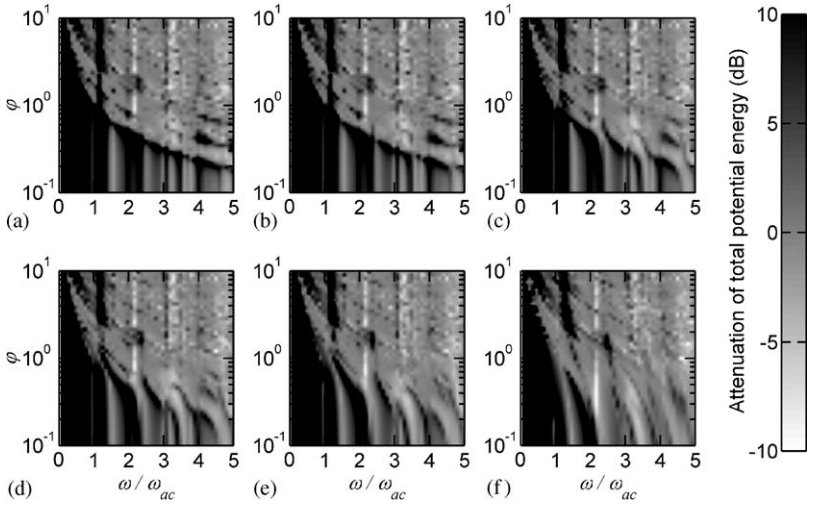

Fig. 2. Maps of overall total acoustic potential energy attenuation under the action of a pure vibration control source at fixed η_c: (a) $\eta_c = 0.01$; (b) $\eta_c = 0.026$; (c) $\eta_c = 0.089$; (d) $\eta_c = 0.162$; (e) $\eta_c = 0.298$; (f) $\eta_c = 1.0$. Error sensor at ($0.7L_{x1}$, $0.7L_{x2}$, $0.9L_{x3}$); force actuator at ($0.495L_{x1}$, 0, $0.481L_{x3}$).

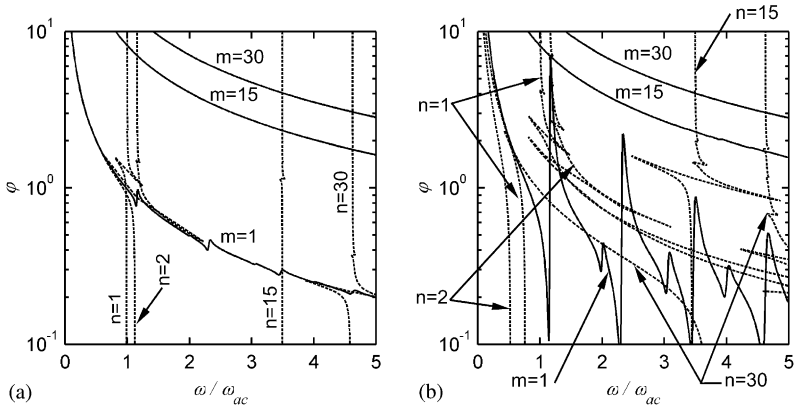

Fig. 3. Schematic diagram of control zones: (a) weak structural–acoustic coupling, $\eta_c = 0.01$; (b) strong structural–acoustic coupling, $\eta_c = 0.30$. ——: line of coupled panel mode frequency; · · · · · ·: line of coupled cavity mode frequency.

some of the localized attenuation at discrete frequencies are meshed out as η_c increases. Besides, it is noticed that the spurious distribution of *PE* attenuation at $\omega > \omega_{ac}$ and small φ becomes more uniform as η_c increases. High *PE* attenuation is usually found around frequencies of modal overlapping (for instance, at $1.16\omega_{ac}$, $2.31\omega_{ac}$, $3.47\omega_{ac}$ and $4\omega_{ac}$). One can find from Eq. (14) that under the cavity-controlled mode, the value of a_n depends critically on the difference between the excitation frequency and natural acoustic mode frequencies of the cavity ω_n at weak structural–acoustic coupling (small η_c). Large a_n will result when the excitation frequency is closed to ω_n. As η_c increases, such effect is reduced, resulting in a more uniform distribution of a_n over the frequency range concerned.

One can again observe from Fig. 2 that all the maps can basically be divided into four zones. A schematic for such division at small η_c is given in Fig. 3a and it can be shown that the zone boundaries are related to the solutions of Eqs. (13) and (15). The nominally vertical dotted lines are some examples of the lines of the coupled cavity eigenfrequencies $\omega_{c,n}$, while the curved solid lines are those for the coupled panel eigenfrequencies $\omega_{c,m}$. The first zone, Zone I, refers to the situation where the excitation frequency ω is less than both $\omega_{c,n=1}$ and $\omega_{c,m=1}$. Very high *PE* attenuation can be found in this region regardless of the values of η_c and φ. Zone II is the region where ω is greater than both $\omega_{c,n=1}$ and $\omega_{c,m=1}$. Again, the *PE* attenuation in this region is not affected by the strength of structural–acoustic coupling very much, though the attenuation map gets a bit more uniform as η_c increases. Also, there are localized high attenuation points at particular eigenfrequencies of the cavity or along the lines of the coupled panel eigenfrequencies. *PE* attenuation is effective at some panel-controlled modes, a few cavity-controlled modes as well as at the combined panel- and cavity-controlled modes. Zone III corresponds to the area where $\omega_{c,m=1} < \omega < \omega_{c,n=1}$ and significant *PE* attenuation can be found at the panel-controlled mode frequencies. Zone IV refers to the region where $\omega_{c,n=1} < \omega < \omega_{c,m=1}$ and the control is found to be effective at the cavity-controlled mode frequencies only.

It can be observed that there are some singularities on the lines shown in Fig. 3a. They are the results of the relatively stronger structural–acoustic mode shape coupling between the panel and the enclosed space at those locations (large value of $C_{n,m}$ in Appendix A). At larger n and m, such

coupling becomes less easy and the lines become smooth (for instance, the line for $\hat{\omega}_{c,m=30}$ and that for $\hat{\omega}_{c,n=30}$).

Fig. 3b shows that the division of the *PE* attenuation map is more complicated at higher value of η_c. The lines of coupled panel eigenfrequencies become very rough for small m. Substantial singularities appear at the frequencies of the cavity modes having nodal plane parallel to the flexible panel when $m = 1$. This is due to the large structural–acoustic mode shape modal coupling factor $C_{n,m}$ between the panel vibration and the cavity resonance. Also, the lines of the coupled cavity eigenfrequencies (Eq. (15)) are significantly curved and some of them consist of two widely separated portions (for example, the lines for $\hat{\omega}_{c,n=1}$ and $\hat{\omega}_{c,n=30}$). The four regions of *PE* attenuation found at small η_c, except Zone I, can hardly be identified (Figs. 2e, f and 3b). It is due to the more uniform distribution of a_n across the frequency range concerned, the chaotic variations of the coupled-controlled mode frequency lines and the effect of the relatively large φ region in Zone IV which eventually make the boundary between Zones II and IV indistinguishable at large η_c.

Two other points can be noticed from Fig. 3. First at large η_c, the lines for $\hat{\omega}_{c,n=2}$ appear closer to the φ axis than those for $n = 1$. It is due to the much larger amplitude of the reactance of $\hat{Y}_{cs,n=2}$ than those for $n = 1$ in the present example. Second, it is observed that the line for $\hat{\omega}_{c,n=15}$ in Fig. 3b consists of an initial straight vertical portion similar to the lines of coupled cavity eigenfrequencies shown in Fig. 3a. In fact, such phenomenon appears whenever the value of n is just higher than the one with a large structural–acoustic mode shape coupling with the $m = 1$ panel mode and the structural–acoustic mode shape coupling of the nth acoustic mode is weak for nearly all panel modes. There are many lines like this and the line for $\hat{\omega}_{c,n=15}$ in Fig. 3b is just an example. The strong singularity along this line is due to the large value of $C_{15,7}$ (large structural–acoustic mode shape coupling). In general, all the singularities and discontinuities of the lines of coupled mode frequencies are due to large structural–acoustic mode shape coupling between the panel and the enclosed cavity.

Fig. 4 illustrates the effects of η_c and the excitation frequency on *PE* attenuation at fixed values of φ. It suggests that the *PE* attenuation does not depend much on the strength of the structural–acoustic coupling for small or large φ (Figs. 4a and f, respectively). Some effects of the coupling are observed in the range $0.2 < \varphi < 1$, but their occurrence is usually restricted to the higher η_c side. Fig. 4 re-iterates the effectiveness of the active control at low frequencies. It should be noticed that strong structural–acoustic coupling (that is, large η_c) will amplify the importance of cavity and/or panel damping effects in the sound transmission process. It can be observed from Eqs. (12) and (14) that the increase in η_c at fixed cavity/panel damping ($\hat{Z}_{ca,m}$ and $\hat{Y}_{cs,n}$, respectively) reduces the values of b_m and a_n, respectively. The effectiveness of the active control will then be reduced as the sound transmission is already effectively controlled by passive means.

4.2. Pure acoustic control

In general, the application of a pure acoustic secondary source in the active control can produce a more uniform *PE* attenuation over the range of φ and frequency at small η_c as shown in Fig. 5a. However, its performance within Zones I, III and IV is worse than that achieved under the pure vibration control, but some improvements can be found at frequencies closed to the cavity eigenfrequencies in Zone II. The four zones of control are less distinctive, especially Zones II and

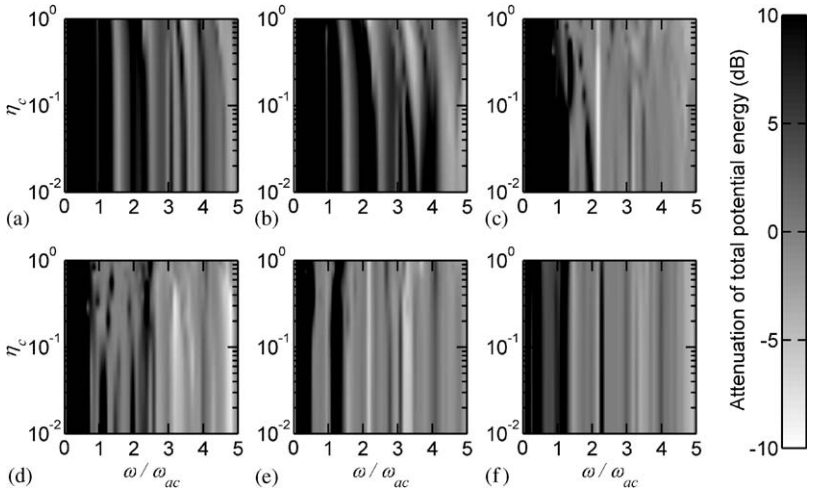

Fig. 4. Maps of overall total acoustic potential energy attenuation under the action of a pure vibration control source at fixed φ: (a) $\varphi = 0.1$; (b) $\varphi = 0.264$; (c) $\varphi = 0.886$; (d) $\varphi = 1.62$; (e) $\varphi = 2.976$; (f) $\varphi = 10$. Error sensor at ($0.7L_{x1}$, $0.7L_{x2}$, $0.9L_{x3}$); force actuator at ($0.495L_{x1}$, 0, $0.481L_{x3}$).

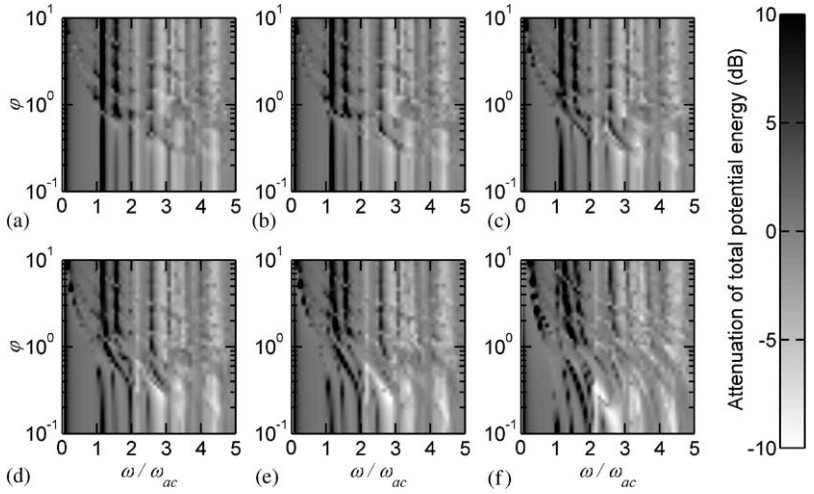

Fig. 5. Maps of overall total acoustic potential energy attenuation under the action of a pure acoustic control source at fixed η_c. Acoustic source at (L_{x1}, L_{x2}, L_{x3}). Other legends: same as those for Fig. 2.

IV at high frequencies. As the strength of the structural–acoustic coupling increases, *PE* amplification gradually appears at lower frequencies and at regions between Zones II and IV. The magnitude of this amplification increases as η_c increases. The active control becomes ineffective in Zone IV when $\eta_c = 1$.

Similar to the case of pure vibration control source, the performance of the active control at small or high φ is again not really affected by η_c except when η_c is closed to unity (Figs. 6a and f). One can observe from Fig. 6c that the pattern is rough at higher values of η_c when φ is closed to unity. This region corresponds to the interface between Zones II and IV in Figs. 5e and f. The

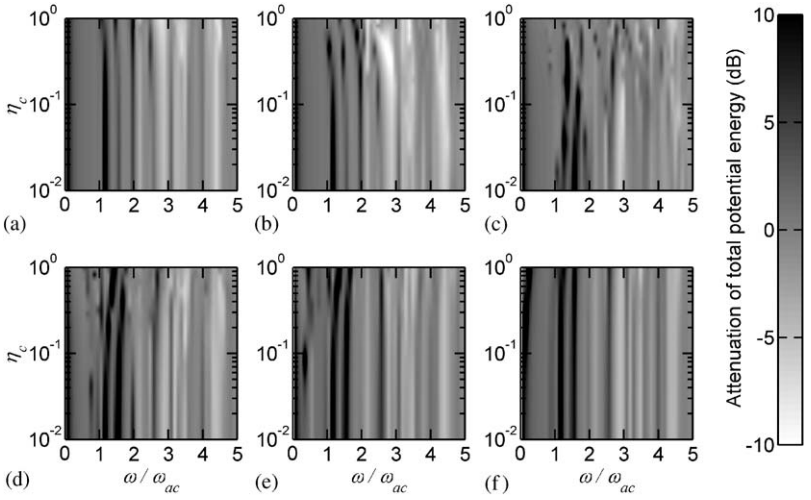

Fig. 6. Maps of overall total acoustic potential energy attenuation under the action of a pure acoustic control source at fixed φ. Acoustic source at (L_{x1}, L_{x2}, L_{x3}). Other legends: same as those for Fig. 4.

pattern in this case is less organized than that in the pure vibration control case, but the localized *PE* amplification at the frequency $2.17\omega_{ac}$ under the pure vibration case (Fig. 4c) is eliminated. One can also find from Fig. 6 that the performance of the active control does not depend much on φ and η_c close to the high end of the frequency range.

In general, the performance of active sound transmission control using a pure acoustic secondary control source is worse than that using the pure vibration control source, especially at low frequencies. The acoustic source tends to increase the chance of having *PE* amplification in the ranges of φ and η_c studied.

4.3. Combined control sources

The combined vibration and acoustic control source system inherits only some of the advantages from the individual control sources. This system enhances the *PE* attenuation at low frequencies significantly (Zone I and some regions in Zone IV) as shown in Fig. 7. However, considerable deterioration of *PE* attenuation can be found at $\varphi > 1$ and $\hat{\omega} > 1.5$, which is a region in Zone II, in the range of η_c studied though some spots of high *PE* attenuation can be found occasionally. Also, some *PE* amplification can be found in Zone III though the control is, in general, enhanced by the combined secondary source system in this control zone. These phenomena are due to the effects of the secondary acoustic source.

The appearance of spots of *PE* attenuation in Zones II and III suggests that this active control is effective at some panel- and cavity-controlled modes. The improvement in the low-frequency range achieved by this combined source control appears to degrade as the strength of the structural–acoustic coupling increases. At small or large φ, the variation of *PE* attenuation with η_c and frequency shows a pattern similar to that obtained under pure vibration control, except that wider attenuation regions (Fig. 8). However, the pattern becomes much less organized when φ is closed to unity as shown in Fig. 8c. One can also observed that the improvement of performance

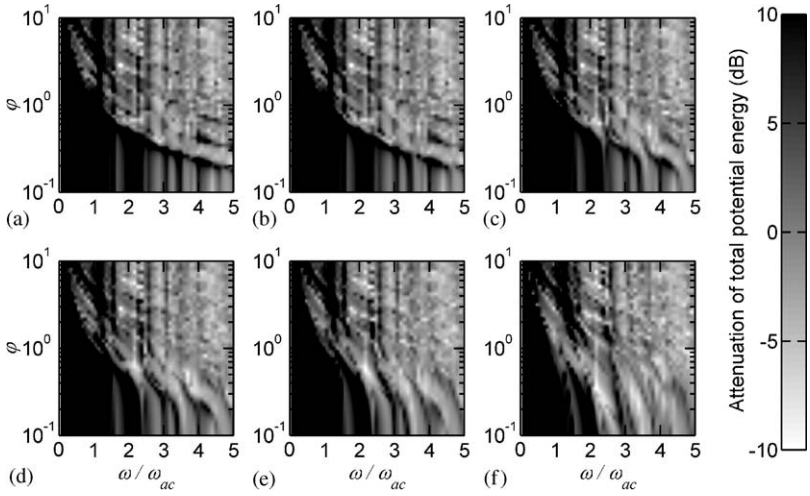

Fig. 7. Maps of overall total acoustic potential energy attenuation under the action of combined acoustic and vibration control sources at fixed η_c. Acoustic source at (L_{x1}, L_{x2}, L_{x3}); force actuator at ($0.495L_{x1}$, 0, $0.481L_{x3}$). Other legends: same as those for Fig. 2.

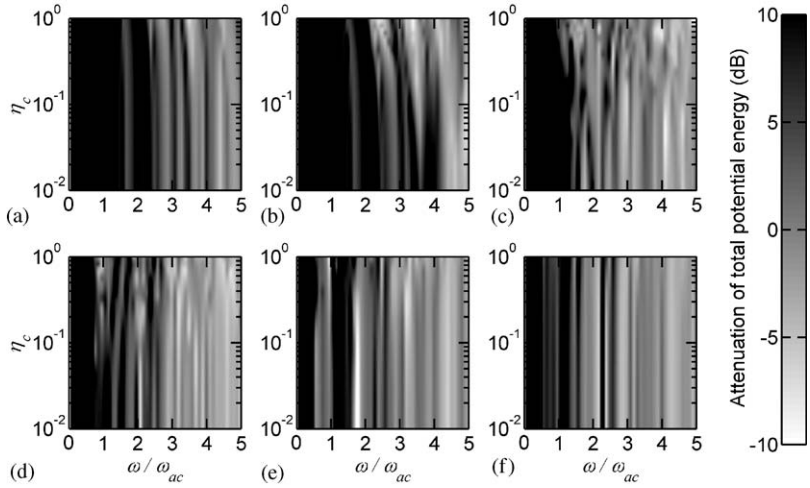

Fig. 8. Maps of overall total acoustic potential energy attenuation under the action of combined acoustic and vibration control sources at fixed φ. Acoustic source at (L_{x1}, L_{x2}, L_{x3}); force actuator at ($0.495L_{x1}$, 0, $0.481L_{x3}$). Other legends: same as those for Fig. 4.

at low frequencies by the present combined source control is not significant when $\varphi > 1$. However, the range $\varphi > 1$ is practically insignificant as it is seldom to have $\omega_{ac} > \omega_{sc}$ in ordinary buildings.

5. Conclusions

The effects of structural–acoustic coupling on the performance of energy density-based active sound transmission control in a slightly damped rectangular enclosed space is investigated

numerically. The performance of energy density control algorithm is described in terms of the overall total acoustic potential energy attenuation resulted from the active control. The frequency range in the present study extends to five times the first eigenfrequency of the cavity. Effects of two dimensionless parameters, namely the strength of structural–acoustic coupling and the ratio between the first eigenfrequencies of the cavity and the panel, are studied. A compact matrix formulation of the steady state optimized secondary source strength for a fully structural–acoustic coupled system under energy density control is derived based on the impedance-mobility approach. Formulae for the coupled panel and cavity eigenfrequencies are derived. The effects of panel impedance and cavity impedance, which are important for passive sound transmission control, are also examined.

The results show that there are four distinct control zones when the structural–acoustic coupling is weak. These regions are separated by the line of first coupled panel eigenfrequency and the line of first coupled cavity eigenfrequency. In the first zone where the excitation frequency is below both the first coupled panel and cavity eigenfrequencies, system with a pure vibration secondary source is very effective in attenuating the overall total acoustic potential energy inside the cavity. The second zone is the region where the excitation frequency is above both the two mentioned coupled eigenfrequencies. Pure vibration source is effective for attenuating some structural modes and a few acoustic modes in this zone but the performance of the active control does not depend much on the strength of the structural–acoustic coupling. When the excitation frequency is between the two mentioned coupled eigenfrequencies, the active control is effective at the panel-controlled modes if the first coupled panel eigenfrequency is lower than the first coupled cavity eigenfrequency. The control becomes effective at the cavity-controlled mode frequencies on the contrary. As the strength of the structural–acoustic coupling increases, these four zones, except those with frequency less than the first coupled cavity eigenfrequency, become less distinguishable.

Active control system with a pure acoustic secondary source produces most uniform performance than that with a pure vibration source over the range of frequency studied. However, the sound attenuation produced by this method is much worse than the vibration source case, especially at low frequencies regardless the strength of the structural–acoustic coupling. Combined vibration and acoustic control source system improves the performance of the active control significantly at low frequency, but tends to deteriorate the performance at high frequencies especially when the excitation frequency is above the first coupled panel eigenfrequency. It is probably due to the acoustic secondary source in the cavity.

In general, the effectiveness of the energy density-based active sound transmission control decreases as the strength of the structural–acoustic coupling increases, due to the increasing damping on the acoustic field inside the cavity and on the vibration of the flexible panel. It also decreases as the ratio between the first eigenfrequencies of the cavity and the flexible panel increases.

Acknowledgements

The financial supports from the Hong Kong Polytechnic University and the Research Grant Council, HKSAR Government are gratefully acknowledged. The advice on material issue from

Dr. C.H. Shek of the Department of Physics and Material Sciences, The City University of Hong Kong is very much appreciated.

Appendix A. Mode shape coupling coefficient and modal decomposition of external force matrix

Sound pressures inside a cavity and structural vibration velocity on the flexible panel can be expressed as Eqs. (1) and (2), respectively, where the complex modal amplitude vectors, **a** and **b**, are given by Eqs. (3) and (4), respectively. They can also be described by the summation of N acoustic and M structural modes, respectively. The acoustic pressure, p, at any point $\mathbf{x}$ inside the cavity and the structural vibration velocity, u_s, at any point $\mathbf{y}$ on the flexible panel can be written as

$$p(\mathbf{x},\omega)=\sum_{n=1}^{N}\psi_n(\mathbf{x})a_n(\omega)=\mathbf{\Psi}^{\mathrm{H}}\mathbf{a} \tag{A.1}$$

and

$$u_s(\mathbf{y},\omega)=\sum_{m=1}^{M}\phi_m(\mathbf{y})b_m(\omega)=\mathbf{\Phi}^{\mathrm{H}}\mathbf{b}. \tag{A.2}$$

For Q number of acoustic source, the complex amplitude of the nth acoustic mode under structural and acoustic excitation is given by [23]

$$a_n(\omega)=Z_{a,n}\left(\sum_{q=1}^{Q}\int_V\psi_n(\mathbf{x})\chi_a(\mathbf{x}_q)\,\mathrm{d}V\cdot q_{c,q}+\int_{S_f}\psi_n(\mathbf{x})u_s(\mathbf{y},\omega)\,\mathrm{d}S_f\right), \tag{A.3}$$

where $\chi_a(\mathbf{x}_q)$ is the acoustic source strength distribution function at $\mathbf{x}_q$ inside the cavity, which is normalized by $q_{c,q}$. For a point acoustic source, $\chi_a(\mathbf{x}_q)=\delta(\mathbf{x}_q)$. The uncoupled acoustic modal impedance, $Z_{a,n}$, is give by

$$Z_{a,n}=\frac{\rho_a c}{V}\left(\frac{\mathrm{j}\omega}{\omega_n^2-\omega^2+2\mathrm{j}\xi_n\omega_n\omega}\right). \tag{A.4}$$

Substituting Eq. (A.2) into Eq. (A.3) gives

$$a_n(\omega)=Z_{a,n}\left(\sum_{q=1}^{Q}D_q(n,q)\cdot q_{c,q}+\sum_{m=1}^{M}C_{n,m}\cdot b_m\right), \tag{A.5}$$

where

$$D_q(n,q)=\int_V\psi_n(\mathbf{x})\chi_a(\mathbf{x}_q)\,\mathrm{d}V, \tag{A.6}$$

$C_{n,m}$ represents the geometric coupling relationship between the uncoupled eigenfunctions of the acoustic modal pressure distribution and the structural modal velocity distribution on the surface of the vibration panel, S_f, and is given by

$$C_{n,m}=\int_{S_f}\psi_n(\mathbf{x})\phi_m(\mathbf{y})\,\mathrm{d}S_f, \tag{A.7}$$

where

$$V = \int_V \psi_n^2(\mathbf{x})\,\mathrm{d}V \quad \text{and} \quad S_f = \int_{S_f} \phi_m^2(\mathbf{y})\,\mathrm{d}S_f, \tag{A.8, A.9}$$

respectively, due to the orthogonal properties of the acoustic and structural mode functions. Thus, the modal acoustic pressure vector, $\mathbf{a}$, can be expressed as

$$\mathbf{a} = \mathbf{Z}_a(\mathbf{D}_q\mathbf{q}_c + \mathbf{q}_s), \tag{A.10}$$

where $\mathbf{q}_s(= \mathbf{Cb})$ is the modal acoustic source strength vector due to vibration of the structure, which acts as a set of acoustic sources on the flexible panel. $\mathbf{D}_q$ is the $N \times Q$ matrix and denotes the couplings between N number of acoustic modes and Q number of acoustic source locations. $\mathbf{C}$ represents the structural–acoustic mode shape coupling relationship between the uncoupled structural and acoustic modes over the surface of the flexible panel. The (n, m) elements of $\mathbf{C}$ is given by Eq. (A.7). $\mathbf{Z}_a$ is an $N \times N$ diagonal matrix defined as the uncoupled acoustic modal impedance matrix. The (n, n) element of $\mathbf{Z}_a$ can be determined by Eq. (A.4).

Similarly, the complex vibration amplitude of the mth structural mode of the flexible panel in Fig. 1 for an isotropic thin plate due to F number of vibration sources and exterior pressure fluctuation on the panel can be expressed as [23]

$$b_m(\omega) = Y_{s,m}\begin{pmatrix} \sum_{f=1}^{F} \int_{S_f} \phi_m(\mathbf{y})\chi_f(\mathbf{y}_f, \omega)\,\mathrm{d}S_f \cdot f_{c,f} \\ + \int_{S_f} \phi_m(\mathbf{y}) p_i(\mathbf{y}, \omega)\,\mathrm{d}S_f \\ - \int_{S_f} \phi_m(\mathbf{y}) p(\mathbf{x}, \omega)\,\mathrm{d}S_f \end{pmatrix}, \tag{A.11}$$

where $\chi_f(\mathbf{y}_f)$ is the vibration source strength distribution function at $\mathbf{y}_f$ on the flexible panel, which is normalized by $f_{c,f}$. For a point force actuator, $\chi_f(\mathbf{y}_f) = \delta(\mathbf{y}_f)$. $p_i(\mathbf{y}, \omega)$ is the exterior acoustic pressure distributions on the surface of the panel. Since the directions of the external force and acoustic pressure are defined to be opposite, there is a minus sign in front of the third integral term in the bracket. The uncoupled structural modal mobility, $Y_{s,m}$, can be expressed as

$$Y_{s,m} = \frac{1}{\rho_s h S_f}\left(\frac{\mathrm{j}\omega}{\omega_m^2 - \omega^2 + 2\mathrm{j}\zeta_m\omega_m\omega}\right). \tag{A.12}$$

Substituting Eq. (A.1) into Eq. (A.11) gives

$$b_m(\omega) = Y_{s,m}(\omega)\left(\sum_{f=1}^{F} D_{f,m} f_{c,f} + g_{p,m} - \sum_{n=1}^{N} C_{n,m}^{\mathrm{T}} \cdot a_n(\omega)\right), \tag{A.13}$$

where

$$D_{f,m} = \int_V \phi_m(\mathbf{y})\chi_f(\mathbf{y}_f, \omega)\,\mathrm{d}V, \tag{A.14}$$

and

$$g_p = \int_{S_f} \phi_m(\mathbf{y}) p_i(\mathbf{y}, \omega)\,\mathrm{d}S_f. \tag{A.16}$$

Thus the modal vibration amplitude vector, $\mathbf{b}$, can be expressed as

$$\mathbf{b} = \mathbf{Y}_s(\mathbf{D}_f\mathbf{f}_c + \mathbf{g}_p - \mathbf{g}_a), \tag{A.17}$$

$\mathbf{g_a} = \mathbf{C}^{\mathrm{T}}\mathbf{a}$ is the modal force vector acting on the acoustic system, which is the reaction force due to the acoustic pressure fluctuation. $\mathbf{D}_f$ is the $M \times F$ matrix and denotes the couplings between M number of structural modes and F number of vibration source locations. $\mathbf{Y}_s$ is the $M \times M$ diagonal matrix defined as the uncoupled structural modal-mobility matrix. The (m,m) element of $\mathbf{Y}_s$ can be determined by Eq. (A.12). The M length vector $\mathbf{g}_p$ is the generalized modal force vector due to the external force distribution $p_i(\mathbf{y},\omega)$. Combining Eqs. (A.10) and (A.17), the acoustic and structural modal amplitude vectors $\mathbf{a}$ and $\mathbf{b}$ can be expressed in terms of the modal excitation vectors $\mathbf{D}_q\mathbf{q}_c$, $\mathbf{D}_f\mathbf{f}_c$ and $\mathbf{g}_p$:

$$\mathbf{a} = (\mathbf{I} + \mathbf{Z}_a\mathbf{C}\mathbf{Y}_s\mathbf{C}^{\mathrm{T}})^{-1}\mathbf{Z}_a(\mathbf{C}\mathbf{Y}_s\mathbf{D}_f\mathbf{f}_c + \mathbf{D}_q\mathbf{q}_c + \mathbf{C}\mathbf{Y}_s\mathbf{g}_p), \tag{A.18}$$

$$\mathbf{b} = (\mathbf{I} + \mathbf{Y}_s\mathbf{C}^{\mathrm{T}}\mathbf{Z}_a\mathbf{C})^{-1}\mathbf{Y}_s(\mathbf{D}_f\mathbf{f}_c - \mathbf{C}^{\mathrm{T}}\mathbf{Z}_a\mathbf{D}_q\mathbf{q}_c + \mathbf{g}_p), \tag{A.19}$$

respectively. Eqs. (A.18) and (A.19) can be re-written as Eqs. (3) and (4), respectively. More details of the derivation can be found in Ref. [14].

In present study of sound transmission problem, an incident plane wave is considered as the primary external source and it excites the structural vibration of the flexible panel. The incident plane wave on the flexible panel outside the cavity at time, t, can be expressed as

$$p_i(\mathbf{r}, t) = P_i e^{j\omega(t-\mathbf{r}/c)}, \tag{A.20}$$

where $\mathbf{r}$ and P_i are the location vector of the observation point and the complex amplitude of the incident plane wave, respectively.

The harmonic incident plane wave on a simply supported plane is considered. Assuming weak coupling between the flexible panel and the external sound field, the mth structural mode of external modal force matrix, $\mathbf{g}_p$, can be written as, according to Roussos [17]

$$g_{p,m} = 4\,S_f P_i I_{m1} I_{m2}, \tag{A.21}$$

where I_{m1} and I_{m2} are resulted from the geometric coupling between the external plane wave and the mth structural mode of flexible plane of dimension $L_{y1} \times L_{y2}$, and

$$I_{m1} = \begin{cases} \dfrac{j}{2}\mathrm{sgn}(\sin\theta\cos\alpha) & \text{for} \quad m_1\pi = \pm\dfrac{\omega L_{y1}}{c}\sin\theta\cos\alpha, \\ \dfrac{m_1\pi[1-(-1)^{m_1}e^{-j(\omega L_{y1}/c)\sin\theta\cos\alpha}]}{[m_1\pi]^2 - [(\omega L_{y1}/c)\sin\theta\cos\alpha]^2} & \text{otherwise}, \end{cases} \tag{A.22}$$

and

$$I_{m2} = \begin{cases} \dfrac{j}{2}\mathrm{sgn}(\sin\theta\sin\alpha) & \text{for} \quad m_2\pi = \pm\dfrac{\omega L_{y2}}{c}\sin\theta\sin\alpha, \\ \dfrac{m_2\pi[1-(-1)^{m_2}e^{-j(\omega L_{y2}/c)\sin\theta\sin\alpha}]}{[m_2\pi]^2 - [(\omega L_{y2}/c)\sin\theta\sin\alpha]^2} & \text{otherwise}. \end{cases} \tag{A.23}$$

Appendix B. Control of η_c and φ

The two dimensionless parameters, η_c and φ, have significant effects on the performance of the active sound transmission control. However, they are not independent of each other. The η_c and φ can be expressed, for the case of rectangular cavity ($L_{x1} \times L_{x2} \times L_{x3}$) with a flexible panel ($L_{y1} \times L_{y2}$), as

$$\eta_c = \left(\frac{c}{\sqrt{D}}\frac{S_f^2}{L_{y1}^2 + L_{y2}^2}\right)\left(\frac{1}{\sqrt{\rho_s h}}\right)\left(\frac{\rho_a S_f}{L_{x2}L_{x3}}\right) = \frac{c}{\sqrt{D}}\frac{L_{x1}^2 L_{x3}^2}{L_{x1}^2 + L_{x3}^2}\frac{L_{x1}}{\sqrt{\rho_s h}}\frac{\rho_a}{L_{x2}\pi^3}, \tag{B.1}$$

and

$$\varphi = \left(\frac{c}{\sqrt{D}}\frac{S_f^2}{L_{y1}^2 + L_{y2}^2}\right)(\sqrt{\rho_s h})\left(\frac{1}{L_{x1}}\right) = \frac{c}{\sqrt{D}}\frac{L_{x1}^2 L_{x3}^2}{L_{x1}^2 + L_{x3}^2}\frac{\sqrt{\rho_s h}}{L_{x1}}\frac{1}{\pi}, \tag{B.2}$$

where h is the thickness of the flexible panel since $L_{y1} = L_{x1}$, $L_{y2} = L_{x3}$ and $L_{x1} > L_{x2}$.L_{x1} is the maximum perpendicular separation between two parallel walls inside the rectangular cavity. The bending stiffness, D, is given by

$$D = \frac{Eh^3}{12(1 - v^2)},$$

where E and v are Young's modulus and the Poisson ratio of the flexible panel. Since the density of media inside the cavity, ρ_a, and the speed of sound is practically fixed. In the present study, the ratios $L_{x2}/L_{x1}(= e/\pi)$ and $L_{x3}/L_{x1}(= 1/\pi)$ are kept constant. Then

$$\frac{\eta_c}{\varphi} = \frac{L_{x1}}{\rho_s h}\frac{\rho_a}{e\pi}.$$

One should note that L_{x1} is allowed to vary and such variation does not affect the results presented in our paper as all length scales in our study are normalized by L_{x1}. For this kind of cavity, since D is proportional to $h^{3/2}$, one finds

$$\eta_c = \frac{L_{x1}^2 K_1}{h^2\sqrt{D'\rho_s}} \quad \text{and} \quad \varphi = K_2\frac{L_{x1}\sqrt{\rho_s}}{h\sqrt{D'}}, \tag{B.3}$$

where $D' = E/12(1 - v^2)$, K_1 and K_2 are constants defined by the aspect ratios of the cavity.

The criterion for cavity i and j of the same aspect ratios to have the same φ is

$$\frac{L_{x1,i}}{h_i}\sqrt{\frac{\rho_{s,i}}{D_i'}} = \frac{L_{x1,j}}{h_j}\sqrt{\frac{\rho_{s,j}}{D_j'}}, \tag{B.4}$$

then

$$\eta_{c,j} = \eta_{c,i}\left(\frac{\rho_{s,i}}{\rho_{s,j}}\right)^{3/2}\sqrt{\frac{D_j'}{D_i'}}. \tag{B.5}$$

In general at a fixed φ, one can reduce η_c by choosing wall material of high density but low Young's modulus. One can also increase η_c by choosing wall material of low density but high

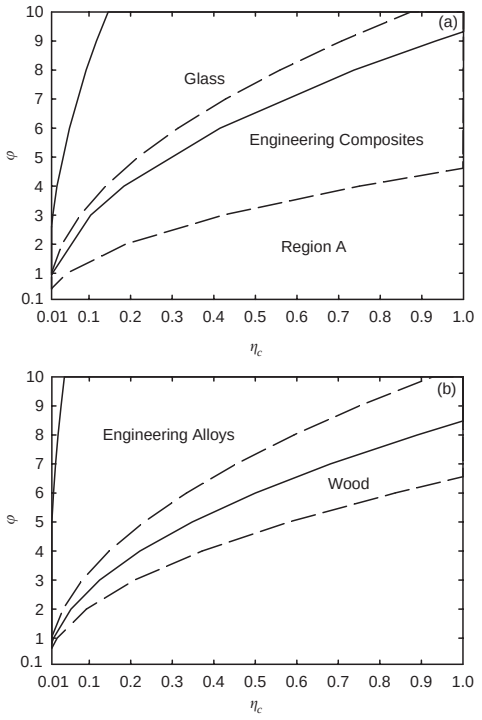

Fig. B1. Regions of φ and η_c for common engineering materials. (a) ———: Boundary for glass; ——: boundary for engineering composites; (b) ———: boundary for engineering alloys; ——: boundary for wood.

Young's modulus. The criterion for cavity i and j of the same aspect ratios to have the same η_c is

$$\frac{L_{x1,i}}{h_i} = \frac{L_{x1,j}}{h_j}\left(\frac{D_i'}{D_j'}\frac{\rho_{s,i}}{\rho_{s,j}}\right)^{1/4}, \tag{B.6}$$

then

$$\varphi_i = \varphi_j\left(\frac{\rho_{s,i}}{\rho_{s,j}}\right)^{3/4}\left(\frac{D_j'}{D_i'}\right)^{1/4}. \tag{B.7}$$

Figs. B1a and b illustrate the ranges of η_c and φ pairs for common engineering materials whose properties are readily found in handbooks and international standards [20–22]. For all the cases presented, $L_{x1}/h > 100$. Though a material cannot be found to fill up region A in Fig. B1a at the time being, the corresponding results are discussed in the present paper for completeness and a believe that such material may currently exist or may be synthesized in the future.

Appendix C. Nomenclature

A structural–acoustic coupling transfer function, $(\mathbf{I} + \mathbf{Z}_a\mathbf{Y}_{cs})^{-1}$ or $(\mathbf{I} + \eta_c\hat{\mathbf{Z}}_a\hat{\mathbf{Y}}_{cs})^{-1}$

B acoustic–structural coupling transfer function, $(\mathbf{I} + \mathbf{Y}_s\mathbf{Z}_{ca})^{-1}$ or $(\mathbf{I} + \eta_c\hat{\mathbf{Y}}_s\hat{\mathbf{Z}}_{ca})^{-1}$

a_n complex acoustic pressure modal amplitude of nth acoustic mode of the enclosure

$\mathbf{a}$ complex acoustic pressure modal amplitude vector, $(N \times 1)$

b_m complex structural vibration velocity modal amplitude of mth structural mode of the flexible panel

$\mathbf{b}$ complex structural vibration velocity modal amplitude vector, $(M \times 1)$

c speed of sound

$\mathbf{C}$ matrix of structural–acoustic mode shape coupling coefficient, $(N \times M)$, $\hat{\mathbf{C}} = \mathbf{C}/S_f$

$\mathbf{D}_f$ couplings between control force actuator locations and structural modes

$\mathbf{D}_q$ couplings between acoustic control source locations and acoustic modes

$\mathbf{f}_c$ vector of vibration control force strengths, $[f_{c,1}\ f_{c,2}\ \ldots]^{\mathrm{T}}$

$\mathbf{g}_p$ external modal force matrix, $(M \times 1)$, $\hat{\mathbf{g}}_p = \mathbf{g}_p/S_f$

$\mathbf{I}$ unit matrix

j $\sqrt{-1}$

k wave number

K_a acoustic bulk stiffness, $\rho_a c^2 S_f^2/V$

M_s mass of the flexible panel

M, N number of structural and acoustic modes respectively

$p(\mathbf{x}, \omega)$ acoustic pressure at $\mathbf{x}$ inside the cavity

$\mathbf{p}$ acoustic pressure vector representing acoustic pressures at discrete points inside the cavity

$\mathbf{q}_c$ vector of acoustic control source strengths, $[q_{c,1}\ q_{c,2}\ \ldots]^{\mathrm{T}}$

$\mathbf{R}_a$ couplings between the control source locations and acoustic modes, $[\mathbf{C}\mathbf{Y}_s\mathbf{D}_f \quad \mathbf{D}_q]$.$\hat{\mathbf{R}}_a = [\hat{\mathbf{C}}\hat{\mathbf{Y}}_s\mathbf{D}_f \quad \mathbf{D}_q]$

$\mathbf{R}_s$ couplings between the control source locations and structural modes, $[\mathbf{D}_f \quad -\mathbf{C}^{\mathrm{T}}\mathbf{Z}_a\mathbf{D}_q]$. $\hat{\mathbf{R}}_s = [\mathbf{D}_f \quad -\eta_c\hat{\mathbf{C}}^{\mathrm{T}}\hat{\mathbf{Z}}_a\mathbf{D}_q]$

S_f area of flexible panel

$\mathbf{t}_c$ control source strengths vector, $[\mathbf{f}_c^{\mathrm{T}}\ \mathbf{q}_c^{\mathrm{T}}]^{\mathrm{T}}$. $\hat{\mathbf{t}}_c = [\mathbf{f}_c^{\mathrm{T}}/S_f\ \mathbf{q}_c^{\mathrm{T}}(\omega_{sc}M_s/S_f^2)]^{\mathrm{T}}$

$u_a(\mathbf{x}, \omega)$ acoustic particle velocity at $\mathbf{x}$ inside the cavity at frequency ω

$u_s(\mathbf{y}, \omega)$ structural vibration velocity at $\mathbf{y}$ on the flexible panel

$\mathbf{u}_s$ structural vibration velocity vector representing structural vibration velocity at discrete points on the flexible panel

V volume of the cavity

$\mathbf{x}$ position vector in the acoustic field inside the cavity, $\mathbf{x} = (x1, x2, x3)$

$\mathbf{y}$ position vector on the flexible panel

$\mathbf{Y}_s$ uncoupled structural modal-mobility matrix, $(M \times M)$ diagonal, $\hat{\mathbf{Y}}_s = (\omega_{sc}M_s)\mathbf{Y}_s$

$\mathbf{Y}_{cs}$ coupled structural modal-mobility matrix, $\mathbf{Y}_{cs}$=$\mathbf{C}\mathbf{Y}_s\mathbf{C}^{\mathrm{T}}$, $\hat{\mathbf{Y}}_{cs} = \hat{\mathbf{C}}\hat{\mathbf{Y}}_s\hat{\mathbf{C}}^{\mathrm{T}}$

$\mathbf{Z}_a$ uncoupled acoustic modal impedance matrix, $(N \times N)$ diagonal, $\hat{\mathbf{Z}}_a = \mathbf{Z}_a\omega_{ac}V/(\rho_a c^2)$

$\mathbf{Z}_{ca}$ coupled acoustic modal impedance matrix, $\mathbf{C}^{\mathrm{T}}\mathbf{Z}_a\mathbf{C}$. $\hat{\mathbf{Z}}_{ca} = \hat{\mathbf{C}}^{\mathrm{T}}\hat{\mathbf{Z}}_a\hat{\mathbf{C}}$

α azimuth angle between the projected plane of the line normal to the external plane wave on the panel and the $x1$-axis

θ incidence angle between the lines normal to the external plane wave and the flexible panel

ρ_a density of media inside the cavity

ρ_s density of flexible panel
ω driving frequency. $\hat{\omega} = \omega/\omega_{ac}$
ω_m mth eigenfrequency of the flexible panel. $\hat{\omega}_m = \omega_m/\omega_{sc}$
ω_n nth eigenfrequency of the acoustic cavity. $\hat{\omega}_n = \omega_n/\omega_{ac}$
ω_{ac} first eigenfrequency of acoustic cavity
ω_{sc} first eigenfrequency of flexible panel
$\omega_{c,m}$ mth coupled panel eigenfrequency. $\hat{\omega}_{c,m} = \omega_{c,m}/\omega_{sc}$
$\omega_{c,n}$ nth coupled cavity eigenfrequency. $\hat{\omega}_{c,n} = \omega_{c,n}/\omega_{ac}$
$\psi_n(\mathbf{x})$ eigenfunction of the acoustic modal pressure distribution inside cavity
$\mathbf{\Psi}$ acoustic mode shape matrix ($N \times d$) for d number of specified points inside cavity
$\phi_m(\mathbf{y})$ eigenfunction of the structural modal velocity distribution on the flexible panel
$\mathbf{\Phi}$ structural mode shape matrix ($M \times d$) for d number of specified points on the flexible panel
ξ_n damping coefficient of nth acoustic mode
ζ_m damping coefficient of mth structural mode

Superscript

$\hat{}$ normalized variable
T transpose
H hermitian transpose

Subscript

c coupled eigenfrequency
m mth structural mode of the flexible panel
n nth acoustic mode of the cavity

References

[1] C.R. Fuller, J.D. Jones, Experiments on reduction of propeller induced interior noise by active control of cylinder vibration, Journal of Sound and Vibration 112 (1987) 389–395.
[2] J. Pan, C.H. Hansen, D.A. Bies, Active control of noise transmission through a panel intro a cavity: I. Analytical study, Journal of the Acoustical Society of America 87 (1990) 2098–2108.
[3] J. Pan, C.H. Hansen, Active control of noise transmission through a panel into a cavity: II. Experimental study, Journal of the Acoustical Society of America 90 (1991) 1488–1492.
[4] J. Pan, C.H. Hansen, Active control of noise transmission through a panel into a cavity: III. Effect of the actuator location, Journal of the Acoustical Society of America 90 (1991) 1493–1501.
[5] X.J. Qiu, J.Z. Sha, J. Yang, Mechanisms of active control of noise transmission through a panel into a cavity using a point force actuator on the panel, Journal of Sound and Vibration 182 (1995) 167–170.
[6] B.S. Cazzolato, C.H. Hansen, Active control of sound transmission using structural error sensing, Journal of the Acoustical Society of America 104 (1998) 2878–2889.
[7] A. Sampath, B. Balachandran, Active control of multiple tones in an enclosure, Journal of the Acoustical Society of America 106 (1999) 211–225.
[8] S.M. Kim, M.J. Brennan, Active control of harmonic sound transmission into an acoustic enclosure using both structural and acoustic actuators, Journal of the Acoustical Society of America 107 (2000) 2523–2534.
[9] S.D. Snyder, C.H. Hansen, The design of systems to control actively periodic sound transmission into enclosed space. Part I: analytical models, Journal of Sound and Vibration 170 (1994) 433–449.

[10] S.D. Snyder, C.H. Hansen, The design of systems to control actively periodic sound transmission into enclosed space, Part II: mechanisms and trends, Journal of Sound and Vibration 170 (1994) 451–472.
[11] S.K. Lau, S.K. Tang, Sound field in a slightly damped rectangular enclosure under active control, Journal of Sound and Vibration 238 (2000) 637–660.
[12] S.D. Sommerfeldt, P.J. Nashif, A comparison of control strategies for minimizing the sound field in enclosures, Proceedings of the Noise-Con 91, 1991, pp. 299–306.
[13] S.D. Sommerfeldt, P.J. Nashif, An adaptive filtered-x algorithm for energy-based active control, Journal of the Acoustical Society of America 96 (1994) 300–306.
[14] S.M. Kim, Active Control of Sound in Structural–Acoustic Coupled Systems, Ph.D. Thesis, University of Southampton, United Kingdom. 1998.
[15] S.M. Kim, A compact matrix formulation using the impedance and mobility approach for the analysis of structural–acoustic systems, Journal of Sound and Vibration 223 (1999) 97–113.
[16] P. Joseph, S.J. Elliott, P.A. Nelson, Statistical aspects of active control in harmonic enclosed sound fields, Journal of Sound and Vibration 172 (1994) 629–655.
[17] L.A. Roussos, Noise transmission loss of a rectangular plate in an infinite baffle, NASA Technical Report 2398, 1985.
[18] P.A. Nelson, A.R.D. Curtis, S.J. Elliott, A.J. Bullmore, The active minimization of harmonic enclosed sound field. Part I: theory, Journal of Sound and Vibration 117 (1987) 1–13.
[19] J.W. Parkins, J. Tichy, A comparison of two active control methods through an investigation of node structures, Proceedings of the ACTIVE 99, Vol. 2, 1999, pp. 729–740.
[20] J.F. Shackelford, W. Alexander, CRC Materials Science and Engineering Handbook, CRC Press, Boca Raton, FL, 2001.
[21] M.F. Ashby, Materials Selection in Mechanical Design, Butterworth-Heinemann, Oxford, 1999.
[22] J.E. Mark, Physical Properties of Polymers Handbook, American Institute of Physics, New York, 1996.
[23] E.H. Dowell, G.F. Gorman III, S.A. Smith, Acoustioelasticity: general theory, acoustic modes and forced response to sinusoidal excitation, including comparisons with experiment, Journal of Sound and Vibration 52 (1977) 519–542.